Preprint, under review in Int. J. Rock Mechanics and Mining Sciences, Aug. 22, 2019

MULTI-PARAMETRIC VARIABLES OF DYNAMIC FAULT MECHANICS

Ze'ev Reches, University of Oklahoma, reches@ou.edu

ABSTRACT

The behavior of faults under dynamic loading reflects the response of the shape and composition of the fault to the applied mechanical loading and environmental conditions. The interaction between the fault properties and the loading system is controlled by multiple variables that may generate an inherently complex behavior. The usage of multi-parametric variables can illuminate the controlling mechanisms of fault dynamic, and here, we describe and evaluate five such variables with presentation of their effectiveness.

1. INTRODUCTION

Faults slip under wide range of loading and environmental conditions that strongly control the fault dynamic slip style, strength, and properties. Major efforts have historically been devoted to characterize the dependency of the dynamic slip on the loading conditions. For example, the dynamic strength of experimental faults revealed systematic dependence on the experimentally applied slip-velocity for cases of constant velocity loading[1,2], and cases of stepping velocity loading[3,4]. The impact of slip-velocity on the dynamic strength is attributed to activation of thermal and mechanical processes[5, 6], but the dynamic strength depends also on the effective normal-stress, evolution of slip-velocity, fault composition, water presence, slip-distance, and other conditions. Thus, while using a single parameter, e.g., slip-velocity, simplifies the analysis, the understanding of fault dynamics requires integration of multiple parameters[1, 2].

It is shown here that multi-parametric variables (MPV) extends the interpretation of experimental observations, and leads to a better insight of fault dynamics than a single-parametric variable. The five MPV of Table 1 are described below, and their significance for fault dynamics interpretation appear in the cited publications.

Table 1. List of multi-parametric variables, which are related to slip-velocity, that control dynamic behavior of experimental, brittle faults. Variable and sources are discussed in the text.

MPV of experimental faults dynamic			Experimental observations	Theory/model
Name	Equation	SI units		
Power-density	$\tau \cdot V$	MW/m^2	Fault dynamic strength	Frictional heating
PV-factor	$\sigma_n \cdot V$	MW/m^2	Slip-system damage	Damage
Impulse-density	τ / V or σ_n / V	MNs/m^3	Wear-rates of brittle faults	Dynamic fracturing
Weakening distance	$\sigma_n \cdot V^{0.5}$	$MPam^{0.5}/s^{0.5}$	Critical slip-distance for melting weakening	Thermal weakening
Kinematic-load	$\int (V \cdot D)\, dt$	m^2/s	Fault response for variable high velocity	Empirical

2. MULTI-PARAMETRIC VARIABLES

2.1 MAPPING MPV

We first demonstrate the need for MPV. Experimental observations indicate that wear-rates and dynamic friction coefficient depend on both slip-velocity, V, and normal-stress, σ_n [7]. An effective method to display this dual dependency is plotting the experimental data in a σ_n - V space[8, 9] (Fig. 1). Boneh and Reches[10] mapped values of friction coefficients and wear-rates data compiled from multiple experimental series (Fig. 1). The maps show that both friction and wear-rate depend on normal stress and slip velocity, yet, the dependence trends differ: The carbonate friction drops for increasing normal stress (Fig. 1A), whereas the wear-rate increases with increasing normal stress (Fig. 1B). This difference illuminates the puzzling relations between rock friction and rock wear-rate[10]. The maps can be used to display theoretical trends and transition zones. For example, Fig. 1A of friction coefficients of carbonate faults, includes two lines of constant PV factor, and Fig. 1B of wear-rates of carbonate, granites and sandstones faults, includes two lines of constant impulse-density. The theoretical mechanical significance of the PV-factor and impulse-density[10] are discussed later. Other published examples include maps of the dynamic friction coefficients in σ_n - V space that reveal weakening and strengthening trends of granite faults[11], and maps of the dynamic friction strength in a displacement-velocity space (D-V) that reveal strength trends of talc gouge layer[12].

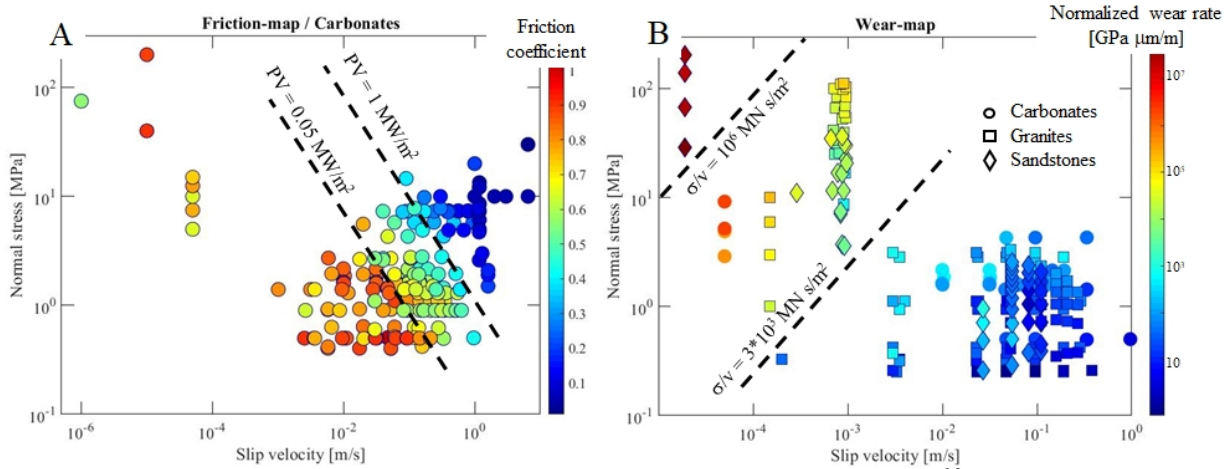

Fig. 1. Geotribological data presented in normal stress–slip velocity space[10]. A. Dynamic, steady-state friction coefficients of carbonates rocks sheared under constant slip-velocity (color scale on the right); dashed lines indicate constant PV-factor (see text). B. Experimental, normalized wear-rates of carbonate, granite, and sandstone faults with two dashed lines of constant (σ/V) divide the data into three groups of wear-rate intensity that include mixed lithologies (see text).

2.2 POWER-DENSITY

Boneh et al.[7] determined the friction coefficients of three types of carbonate faults that were sheared under constant slip-velocity. The plotted steady-state friction coefficients, μ, as function of the experimental normal stress displayed wide scatter (Fig. 2A), but once the μ data are divided into three velocity groups (V<0.1 m/s, V=0.1–0.3 m/s, and V>0.3m/s), it emerged that μ decreases with the increase of both normal stress and slip-velocity. The scatter disappears for the same friction data as function of power-density, PD (Fig. 2B), where

$$PD = [\text{shear stress} \cdot \text{slip velocity}] = \tau \cdot V$$

in which τ is the shear stress and V is the slip velocity (Table 1). Another example of the effectiveness of power-density was presented experiments on granitic faults sheared at constant velocity[13]. In this study[13], the plot of the steady-state friction coefficients as function of slip velocity revealed no systematic relations, but the same friction data plotted as function of power-density displayed systematic, yet non-trivial relationships.

Power-density is a rational parameter to affect fault dynamic friction because PD is the dissipation rate of mechanical energy per unit area of the shearing fault. The trends in Fig. 2 strengthen the significance of PD. As both PD and μ depend linearly on the shear-stress, τ, it is expected to observe a positive dependence between the two parameters; however, the experimental data indicate negative dependence for carbonate faults (Fig. 1B) and non-monotonic dependence for granitic rocks[13, 14]. The power-density is probably the best estimate of the rate of frictional heating during shear. This issue was investigated by Siman-Tov et al.[15, 16] who

attributed the dynamic weakening and formation of mirror surfaces along carbonate faults to thermally-activated processes. They used the measured power-density as the sole heat source, and converted the mechanical work into conducted heat. The modeled temperature evolution is in very good agreement with the experimentally-measured temperatures.

A related parameter to the power-density is the PV-factor of engineering tribology that was mentioned above (Fig. 1A)[17, 18]. The PV-factor is the product of pressure, P, and velocity, V. It is used to quantify the expected damage resistance of a frictional system that may not be loaded above a critical PV-factor[19]. The similarity between PD and PV,

$$PV = \sigma_n \cdot V = \tau \cdot V / \mu = PD / \mu,$$

allows for a useful application of the PV-factor to shear experiments along rock faults[10]. In these experiments the normal stress, σ_n, is practically constant while the shear stress, τ, evolves by the dynamic response of the fault. Thus, in a constant velocity experiment, the PV-factor defines a constant load setting, unlike the PD that varies with displacement. The two lines of constant PV (0.05 and 1.0 MW/m^2) in Fig. 1A divide the experimental friction data into three fields of dynamic frictional strength which are controlled by the loading intensity PV.

Finally, the power-density, PD, is a measure of the rate of frictional energy dissipation per unit area during fault slip[15, 16]. The rate of energy dissipation on the fault, PD, is bounded by rate of energy flow to the fault, which is the energy-flux. This correspondence between PD and energy-flux suggest demonstrate that the intensity of energy-flux may control the slip-velocity and the slip style of a fault[20], and it was shown that low energy-flux yields stable, constant velocity, whereas high energy-flux yields unstable, stick-slips[20].

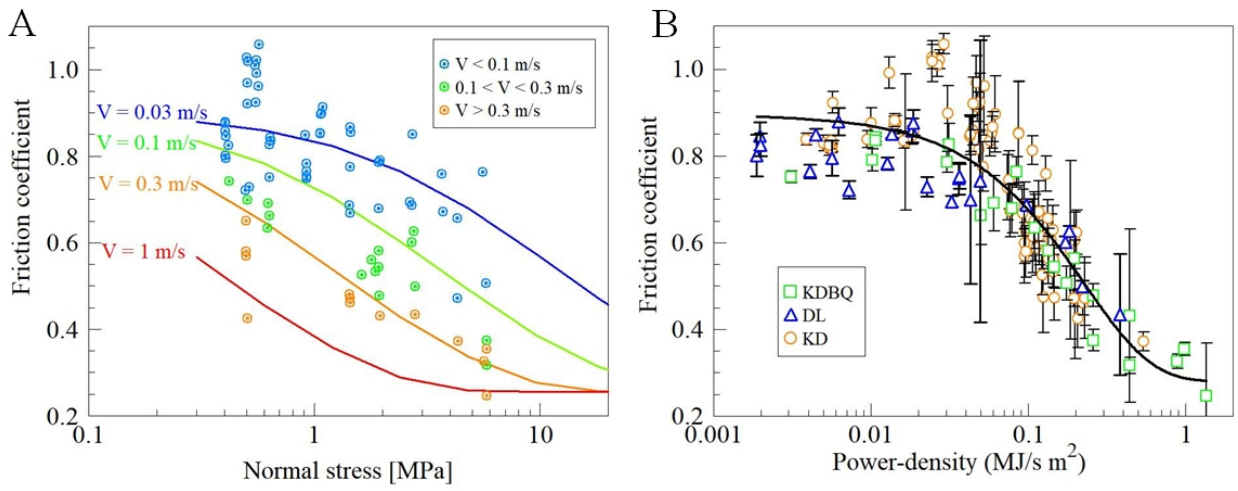

Fig. 2. A & B. Steady-state, dynamic friction coefficients of three types of carbonate faults[7]. Data are plotted as function of experimental normal stress and divided into three groups of slip-velocity (A), and as function of power-density with best fit (black curve) of $\mu = 0.28+0.61 \cdot 0.012^{PD}$.

2.3 IMPULSE DENSITY AND FAULT WEAR

Early investigations of fault wear[21] adopted the classic Archard equation[22] which states that the wear-rate, WR, during slip is

$$WR = W / D = K \cdot (\sigma_n/H)$$

where W is wear amount, D is slip-displacement, K is a material constant, σ_n is the normal stress, and H is the material hardness. While Archard equation fits wear data of industrial materials, the wear of brittle rock strongly depends on the slip-velocity[7, 23], and this variable is ignored in Archard equation. The compilation of wear-rate data from seven steady-state experimental series[10] of faults composed of granites, carbonates, and sandstones, indicated systematic relationship to the experimental ratio (τ / V) over 6-7 orders of magnitude (Fig. 3). Boneh and Reches[10] modeled the wear mechanics by assuming that brittle faults wear by fracturing of highly stressed, contacting asperities[24]. They further postulated that the fracturing is controlled by the loading rate as brittle materials are stronger under high loading rates[25, 26]. By linking the loading rate to the slip-velocity, it was shown that the asperity strength is proportional to the mechanical impulse, which is the product of force, F, and loading period Δt[10]. This analysis showed that the wear-rate, WR, for a brittle fault is

$$WR \cdot H = K \cdot (\tau/V)$$

where (τ / V) is the mechanical-impulse density, H is the hardness of the fault rock and K is a constant of unit scaling. Normalization of the data (experimental wear-rate times fault hardness, WR·H), yielded a universal wear-rate dependency on the impulse-density as shown in Fig. 3.

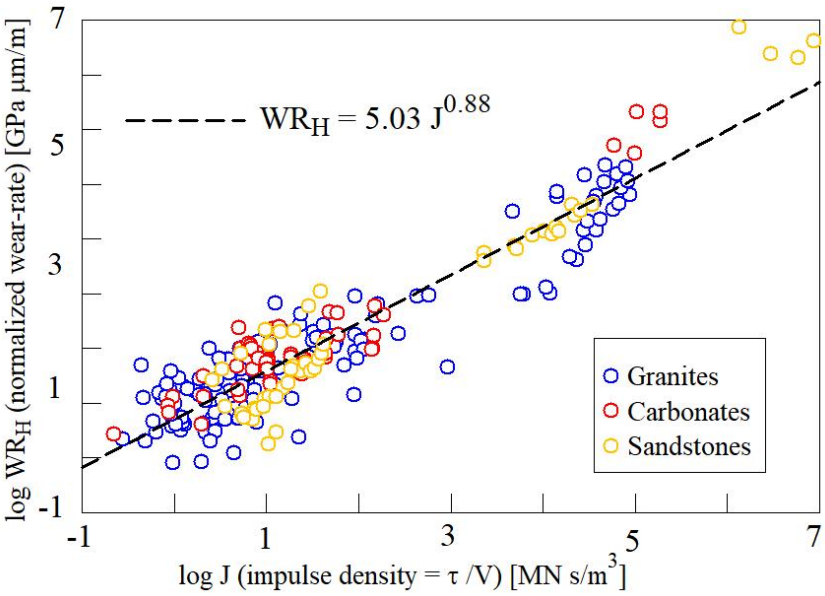

Fig. 3. Normalized wear-rates (measured wear-rate x hardness) for three rock types, granites, carbonates and sandstones[10]

.2.4 KINEMATIC LOAD

A recent investigation[27] of the frictional properties of fault gouge was conducted on samples collected at three field sites along the Alpine Fault, New Zealand. The experiments focused on seismic slip at shallow depth with original gouge as-well-as mixed gouge samples. The gouge layers were sheared under low normal stress (2-3 MPa), and subjected to six steps of cyclical slip-velocity ranging from 0.002 to 1.47 m/s with maximum slip-displacement of 10.2 m. The

authors observed episodes of drastic gouge weakening that were associated with marked temperature rises and intense CO_2 and H_2O emissions. The analysis showed that the gouge deformation indicators, including dynamic friction coefficient, temperature, gouge compaction, and CO_2 emission, were related to both the temporal slip-velocity during the steps and the cumulative slip-displacement of the run[27]. The authors presented the results as separate dependencies on slip-velocity and on slip-displacement.

We think that the separated dependencies approach misses the apparent recognition that the response of the gouge layers was to a combined effect of the slip-velocity, V, and slip-displacement, D. Accordingly, we propose a new variable termed here 'kinematic-load', KL,

$$KL = \int (V \cdot D)\, dt$$

that correlates the gouge behavior at time t to the ingrated product V·D up to this time. The application of the measured kinematic-load to the gouge behavior data of Chen at al. (2019)[27] reveals systematic dependence on KL, with similar trends for all measured deformation indicators (Fig. 4). We envision that the kinematic-load variable represents the integrated effects of V and D in cases of changes in slip-velocity with time, and as fault slip during a natural earthquake is always associated with intense variations of slip-velocity[28], the kinematic-load variable may help evaluating the dynamic behavior of rupturing faults.

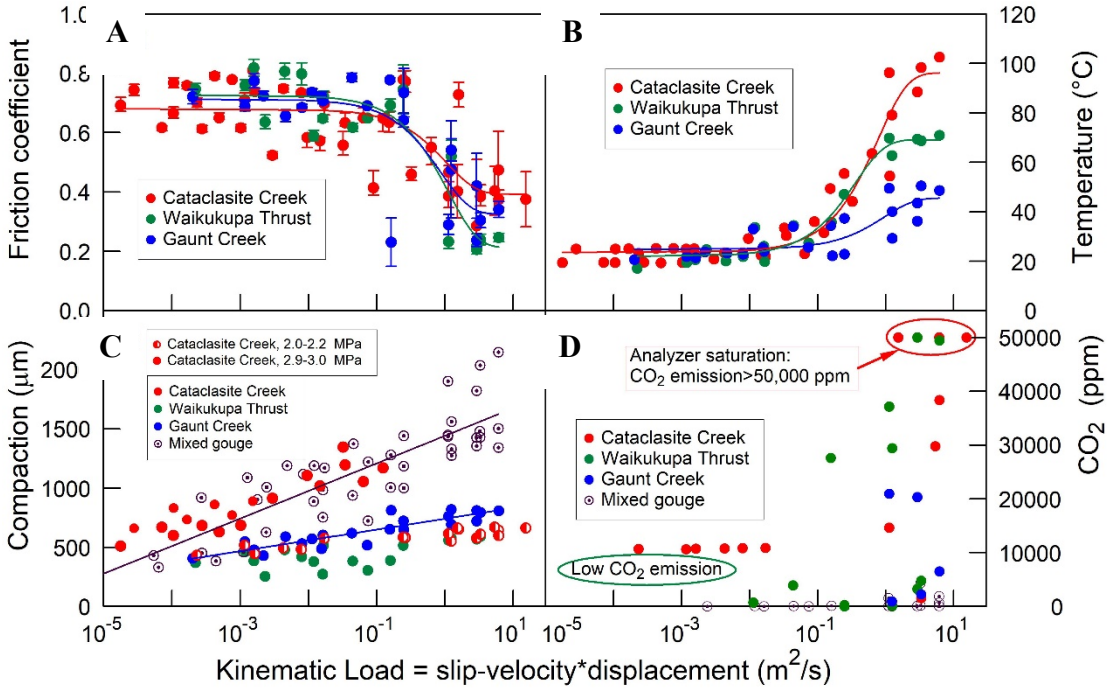

Fig. 4. Synthesis of experimental observables Alpine fault gouge sheared at cyclical stepping velocity[27]. Data plotted as function of kinematic-load, KL (text), including dynamic friction coefficients (A), fault zone temperature (B), fault-normal compaction (C), and CO_2 emission (D). The fitted curves illustrate the evolution trends of the monitored parameters.

2.5 WEAKENING DISTANCE DURING FAULT SLIP

Many experimental analyses revealed complex evolution of the frictional strength during slip along faults composed of igneous rocks, e.g., granites and gabbros[5, 2, 29, 30]. The strength evolution includes three general stages (Fig. 5A)[11]: I. Weakening associated with brittle fragmentation and powder lubrication; II. Strengthening associated with partial melting and viscous braking; and III. Final weakening associated with the formation of continuous melt layer along the fault surface after slip-distance, D_t. Niemeijer et al. (2011)[2] investigated the transition to the final weakening stage of low-viscosity, melt film, and assumed that it is related to a temperature rise above a critical threshold that is related to the fault composition. They recognized that this thermal transition is controlled by the evolving, complex power-density evolution during stages I and II (Fig. 5A). Niemeijer et al. (2011)[2] realized that due to the complex evolution "…no simple theoretical argument can be made…" to predict D_t, and they followed an empirical fit in which

$$D_t = b \cdot (\sigma_n \cdot V^{1/2})^{-a}$$

where a and b are constants, and a is close to 1. This variable fits the experimental observations of gabbro faults[2] that were sheared under wide range of slip-velocity and normal stress (black line in Fig. 5B). The effectiveness of this equation for the slip-distance weakening, D_t, was further tested for granitic faults that were sheared and melted (Fig. 5B)[11]. The granitic faults have the same characteristic dependence of D_t on $(\sigma_n \cdot V^{1/2})$, but with a constant b ~ 8 (red line in Fig. 5B), instead of b ~ 50.5 for gabbro fault (black line in Fig. 5B). This difference of b values may reflect the composition difference of critical melting thresholds between gabbro and granite[11].

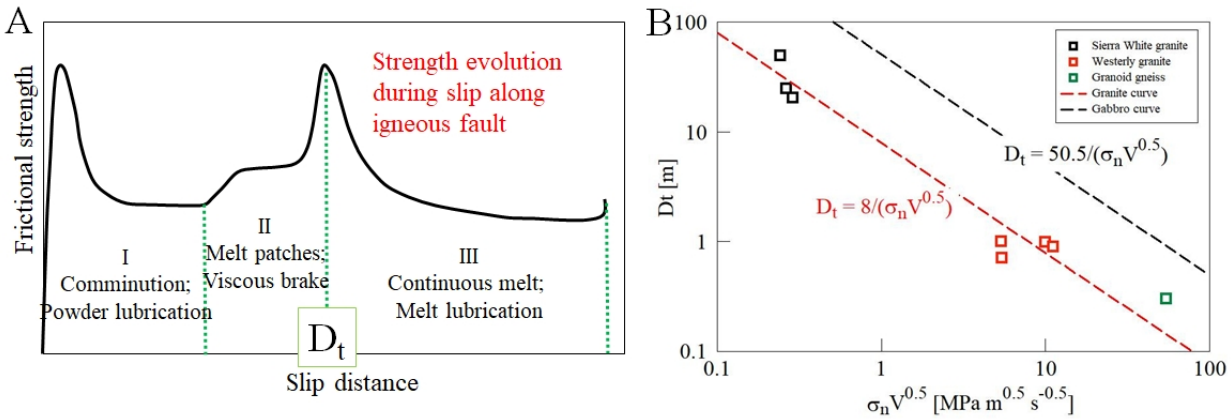

Fig. 5. A. Schematic evolution of the dynamic frictional strength during shear along igneous faults with three stages of strength evolution[11]. B. The weakening distance, Dt, for the transition from Stage II to III (A) into low viscosity shear along a melt film (text). The data include experimental results of granitic faults (square symbols), calculated data fit for the granites (red line)[11], and calculated curve for gabbro faults[2] (black line) (see text).

3. ACKNOWLEDGMENTS

The present work is based on the invaluable contributions of Yuval Boneh, Brett Carpenter, Xiaofeng Chen, and Zonghu Liao, whose collaboration and data sharing are greatly appreciated. Discussions with Yonathan Reches helped to illuminate central key points. Many thanks to these researchers who do not necessarily share the views expressed here. Partial support was provided by NSF grant EAR-1620330 "Investigating Earthquake Source Processes in the Laboratory" and NSF grant EAR-1345087 "Experimental simulation of earthquake rupture processes".

4. REFERENCES

1 Di Toro, G, Han R, Hirose T, De Paola N, Nielsen S, Mizoguchi K, Ferri F, Cocco M, Shimamoto T. Fault lubrication during earthquakes. *Nature* 471, 7339, 2011: 494.

2 Niemeijer A, Di Toro G, Nielsen S, Di Felice F. Frictional melting of gabbro under extreme experimental conditions of normal stress, acceleration, and sliding velocity. J Geoph. Res., Solid Earth, 2011; 116.

3 Dieterich, JH. Modeling of rock friction: 1. Experimental results and constitutive equations. J of Geoph. Res., Solid Earth,1979; 84, 2161–2168.

4 Scholz, C. H. (1998). Earthquakes and friction laws. *Nature*, *391*(6662), 37.

5 Hirose T, Shimamoto T. Growth of molten zone as a mechanism of slip weakening of simulated faults in gabbro during frictional melting. *J Geoph. Res., Solid Earth,* 2005; 110, B05202. https://doi.org/10.1029/2004JB003207

6 Rice, J. R. (2006). Heating and weakening of faults during earthquake slip. *J Geoph. Res., Solid Earth*, 111, B05311. https://doi.org/10.1029/2005JB004006

7 Boneh Y, Sagy A, Reches Z. Frictional strength and wear-rate of carbonate faults during high-velocity, steady-state sliding. *Earth Planet. Sci. Lett.,* 2013; 381, 127-137.

8 Vingsbo, O., & Söderberg, S. On fretting maps. Wear, 1988; 126, 131-147.

9 Wang DZ, Peng HX, Liu J, Yao CK. Wear behavior and microstructural changes of SiCW–Al composite under lubricated sliding friction. *Wear*, 1995; 184, 187–192.

10 Boneh Y, Reches Z. Geotribology-Friction, wear, and lubrication of faults. *Tectonophysics,* 2018; 733, 171-181.

11 Chen X, Madden ASE, Reches Z. Friction evolution of granitic faults: Heating controlled transition from powder lubrication to frictional melt. *J Geoph. Res., Solid Earth,* 2017a; 122, 9275-9289.

12 Chen X, Madden ASE, Reches Z. The frictional strength of talc gouge in high-velocity shear experiments. *J Geoph. Res., Solid Earth,* 2017b; 122, 3661-3676.

13 Liao Z, Chang JC, Reches Z. Fault strength evolution during high velocity friction experiments with slip-pulse and constant-velocity loading. *Earth Planet. Sci. Lett.* 2014; 406, 93–101.

14 Reches Z, Lockner DA. Fault weakening and earthquake instability by powder lubrication. *Nature,* 2010; 467, 452–455. https://doi.org/10.1038/nature09348

15 Siman-Tov S, Aharonov E, Boneh Y, Reches Z. Fault mirrors along carbonate faults: Formation and destruction during shear experiments. *Earth Planet. Sci. Lett.,* 2015; 430, 367–376. https://doi.org/10.1016/j.epsl.2015.08.031

16 Siman-Tov S, Aharonov E, Sagy A, Emmanuel S. Nanograins form carbonate fault mirrors. *Geology*, 2013; 41, 703–706. https://doi.org/10.1130/G34087.1

17 Ramalho A, Miranda JC. The relationship between wear and dissipated energy in sliding systems. *Wear*, 2006; 260, 361-367.

18 Williams JA. Wear and wear particles—some fundamentals. *Tribol. Int.,* 2005; 38, 863–870.

19 Wang YA, Li JX, Yan Y, Qiao LJ. Effect of pv factor on sliding friction and wear of copper-impregnated metallized carbon. *Wear,* 2012; 289, 119-123.

20 Reches, Z, Zu, X., Carpenter, BM. Energy-flux control of the steady-state, creep, and dynamic slip modes of faults. Scientific Reports, 2019; 9, 10,627.

21 Wang WB, Scholz CH. Wear processes during frictional sliding of rock – a theoretical and experimental study. *J Geoph. Res., Solid Earth,* 1994; 99, 6789–6799.

22 Archard, J.F., 1953. Contact rubbing of flat surfaces. J. Appl. Phys. 24, 981–988.

23 Hirose T, Mizoguchi K, Shimamoto T. Wear processes in rocks at slow to high slip rates. *J. Struct. Geol.,* 2012; 38, 102–116.

24 Engelder, J., Scholz, C. The role of asperity indentation and ploughing in rock friction—II: Influence of relative hardness and normal load. *Int. J. Rock Mech. Min. Sci. Geomech. Abstr., 1976;* 155–163 Elsevier.

25 Zhang Q, Zhao J. Effect of loading rate on fracture toughness and failure micromechanisms in marble. *Eng. Fract. Mech.,* 2013; 102, 288–309.

26 Zhang Z, Kou S, Yu J, Yu Y, Jiang L, Lindqvist PA. Effects of loading rate on rock fracture. *Int. J. Rock Mech. Min. Sci.*, 1999; 36, 597–611.

27 Chen X, Morgan CB, Carpenter BM, and Reches Z. Weakening mechanisms of Alpine Fault gouge in high-velocity shear experiments. *J of Geoph. Res., Solid Earth,* 2019; (on line).

28 Tinti E, Fukuyama E, Piatanesi A, Cocco M. A kinematic source-time function compatible with earthquake dynamics. *Bull. Seismol. Soc. Am.* 2005; 95, 1211–1223.

29 Shimamoto T, Lin A. Is frictional melting equilibrium melting, or non-equilibrium melting? *J Tectonic Research Group Japan*, 1994; 39, 79–84.

30 Spray JG. Viscosity determinations of some frictionally generated silicate melts: implications for fault zone phenology at high strain rates. *J Geoph. Res., Solid Earth, 1993;* 98, 8053–8068. https://doi.org/10.1029/93JB00020